Article

CYP153A71 from *Alcanivorax dieselolei*: Oxidation beyond Monoterminal Hydroxylation of *n*-Alkanes

Cheri Louise Jacobs [1,2], Rodolpho do Aido-Machado [1], Carmien Tolmie [1], Martha Sophia Smit [1,2] and Diederik Johannes Opperman [1,2,*]

[1] Department of Microbiology and Biochemistry, University of the Free State, Bloemfontein 9300, South Africa
[2] South African DST-NRF Centre of Excellence in Catalysis, c*change, University of Cape Town, Cape Town 7700, South Africa
* Correspondence: opperdj@ufs.ac.za; Tel.: +27-51-401-2714

Abstract: Selective oxyfunctionalization of non-activated C–H bonds remains a major challenge in synthetic chemistry. The biocatalytic hydroxylation of non-activated C–H bonds by cytochrome P450 monooxygenases (CYPs), however, offers catalysis with high regio- and stereoselectivity using molecular oxygen. CYP153s are a class of CYPs known for their selective terminal hydroxylation of *n*-alkanes and microorganisms, such as the bacterium *Alcanivorax dieselolei*, have evolved extensive enzymatic pathways for the oxyfunctionalization of various lengths of *n*-alkanes, including a CYP153 to yield medium-chain 1-alkanols. In this study, we report the characterization of the terminal alkane hydroxylase from *A. dieselolei* (CYP153A71) for the oxyfunctionalization of medium-chain *n*-alkanes in comparison to the well-known CYP153A6 and CYP153A13. Although the expected 1-alkanols are produced, CYP153A71 readily converts the 1-alkanols to the corresponding aldehydes, fatty acids, as well as α,ω-diols. CYP153A71 is also shown to readily hydroxylate medium-chain fatty acids. The X-ray crystal structure of CYP153A71 bound to octanoic acid is solved, yielding an insight into not only the regioselectivity, but also the binding orientation of the substrate, which can be used in future studies to evolve CYP153A71 for improved oxidations beyond terminal *n*-alkane hydroxylation.

Keywords: alkane hydroxylation; cytochrome P450 monooxygenase; oxyfunctionalization; CYP153; hydroxy fatty acids

1. Introduction

The selective oxyfunctionalization of non-activated $C(sp^3)$-H bonds remains a challenge for traditional synthetic chemistry, especially when using molecular oxygen as an oxidant [1]. The biocatalytic hydroxylation of sp^3 carbons has, thus, emerged as a promising alternative due to their ability to activate dioxygen from air under mild-reaction conditions and often unrivalled regio- and stereoselectivity/specificity [2]. Cytochrome P450 monooxygenases (CYPs or P450s) belong to a group of heme-thiolate enzymes able to catalyze the hydroxylation of a diverse set of compounds. As monooxygenases, CYPs require two electrons from NAD(P)H to activate molecular oxygen in the heme center of the enzyme, where a high-valent iron(IV)-oxo cationic radical is formed from one oxygen atom, which in turns hydroxylates the C–H bond, and the second oxygen atom is reduced to water [3].

CYP153s are a family of bacterial CYPs able to hydroxylate the terminal carbon of medium-chain *n*-alkanes [4]. As CYP153s cannot directly bind NAD(P)H, they require auxiliary redox-partner proteins to deliver the electrons for oxygen activation to the heme center. CYP153s belong to class-I CYPs, or the so-called "three-component system", which uses FeS-containing ferredoxin (Fdx) and FAD-containing ferredoxin reductase (FdR) for sequential electron transfer [5]. Genes encoding these redox-partner proteins are generally in close genetic proximity to the CYP153-encoding genes [6], with, in some instances, such

as with CYP153A6 from the *Mycobacterium* sp. strain HXN-1500, all three proteins expressed from a single operon [7,8].

To overcome the higher bond-dissociation energy of the terminal carbon, CYP153s must bind *n*-alkanes in an orientation where only the terminal carbon is accessible to the activated oxygen. The corresponding 1-alkanols can then be oxidized further by alcohol and aldehyde dehydrogenases to fatty acids, which can be utilized as a carbon source through β-oxidation. In addition to their recognized natural function as alkane hydroxylases, based in part on their low dissociation constants for medium-chain *n*-alkanes, most CYP153s display promiscuous activity. Members of the CYP153 family have been demonstrated to catalyze the epoxidation of cyclic and terminal *n*-alkenes [9], epoxidation of styrene [10] and 4-phenyl-1-butene [11], ω-hydroxylation of fatty acids [12] and alkylbenzene [11], as well as the hydroxylation of the terminal methyl group of *p*-cymene and limonene to form *p*-cumenol and perillyl alcohol [7,13], respectively. The over-hydroxylation of primary alcohol products obtained from *n*-alkanes has also been observed [14,15], mainly forming α,ω-diols and aldehydes, typically from longer-chain alkanes as side-products.

Directed evolution has also been used to alter, broaden, or improve the activity of CYP153s. CYP153A7 has been evolved into a highly regio- and enatio-selective sub-terminal hydroxylase, producing (*S*)-2-octanol (>99% *rr*, 98% *ee*) from *n*-octane [16]. The substrate range has also been expanded beyond medium-chain alkanes, with CYP153A34 engineered for the terminal hydroxylation of *n*-butane to 1-butanol [17] and CYP153A7 for the production of 1,4-butanediol from 1-butanol [18]. More recently, the focus has shifted to improving the ω-hydroxylation of fatty acids [12,19–22]. CYP153A33 (CYP153A$_{M.aq}$) was engineered through focused mutagenesis based on structure-sequence alignments to create a variant (M.aqRLT) with a 151-fold improvement in catalytic efficiency for 8-hydroxyoctanoic acid production of [23]. Through a single mutation (D258E), CYP153A7's catalytic efficiency for the terminal hydroxylation of octanoic acid was improved 3.8-fold [24].

Alcanivorax dieselolei strain B-5 can use C_5–C_{36} *n*-alkanes as a sole carbon source. Genomic analysis revealed this activity to be mediated by a set of different complementary alkane hydroxylases working in concert [25,26]. This includes two homologs of integral membrane-bound non-heme iron alkane hydroxylases (AlkBs), a CYP from the CYP153 family, and an AlmA-like (flavin binding) alkane hydroxylase. In this study, we describe the catalytic and structural characterizations of the CYP153 from *A. dieselolei*, compared to the extensively studied CYP153A6 from *Mycobacterium* [25] and the CYP153A13 from *Alcanivorax borkumensis* SK2 [27].

2. Results and Discussion

2.1. Heterologous Expression of CYP153A71 and Associated Redox-Partner Proteins

The previously identified CYP153 obtained from *A. dieselolei* strain B-5, subsequently named CYP153A71, was PCR-amplified and cloned into the pET22b(+) and pET28b(+) vectors for heterologous expression in *Escherichia coli*. The two vectors would provide either the native CYP153A71 (pET22b(+)) or an N-terminal His-tagged variant (pET28b(+)). Genome analysis revealed a ferredoxin (Fdx-A71) directly upstream of CYP153A71 and a ferredoxin reductase (FdR-A71) approximately 1.8 kb downstream of the CYP153A71 gene. The genes encoding these associated redox partners were similarly amplified and cloned for expression in *E. coli*. SDS-PAGE analysis revealed CYP153A71 expressed as soluble proteins from both plasmids (Figure 1a); although FdR-A71 expressed from both vectors did not yield significant quantities of soluble protein. Soluble expression was, however, achieved for both the native and His-tagged variants of Fdx-A71 (Figure 1b). CO-difference spectra were performed to quantify and confirm the correct folding of CYP153A71 and, compared to CYP153A6 from *Mycobacterium* and CYP153A13 from *A. borkumensis* SK2 (49% and 84% amino-acid-sequence identity to CYP153A71, respectively), expressed in *E. coli* from the same vector under similar conditions. Spectral analysis of the cell-free extracts (CFEs)

of all three CYP153s showed 450 nm peaks, with CYP153A71 and CYP153A6 displaying significantly higher expression levels (*ca.* 10–11 μM) than CYP153A13 (*ca.* 4 μM, Figure 1c).
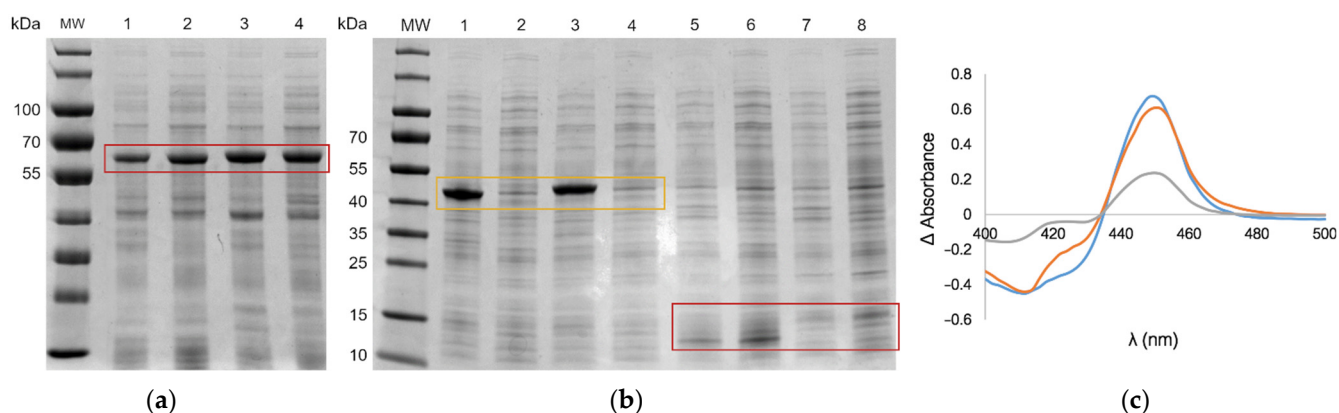

Figure 1. SDS-PAGE analysis of *A. dieselolei* B-5 proteins expressed in *E. coli* BL21-Gold (DE3). (**a**) CYP153A71 expressed from pET22b(+) (lanes 1–2) and pET28b(+) (lanes 3–4); lanes 1 and 3 represent the total crude cell lysate fraction and lanes 2 and 4 the soluble protein fractions (CFEs); (**b**) natural redox partners of CYP153A71; FdR-A71 (lanes 1–4) and Fdx-A71 (lanes 5–8). Lanes 1, 2, 5, and 6 represent redox partners expressed from pET22b(+), and lanes 3, 4, 7, and 8 are redox partners expressed from pET28b(+). Lanes 1, 3, 5, and 7 represent the crude cell lysate fractions and lanes 2, 4, 6, and 8 represent the soluble protein fractions (CFEs). CYP153A71 (54/56 kDa); FdR-A71 (42/44 kDa); and Fdx-A71 (12/14 kDa). MW: PageRuler prestained protein ladder; (**c**) CO-difference spectra obtained using the cell-free extract of CYP153A71 (blue) compared to CYP153A6 (orange) and CYP153A13 (gray).

2.2. Redox-Partner Coupling

In an initial attempt to reconstitute the activity of CYP153A71, 1 mL biotransformation reactions were performed with CYP153A71 coupled to its natural redox partners for the conversion of *n*-octane. Equal volumes (200 μL) of CFEs containing either CYP153A71, Fdx-A71, and FdR-A71 were mixed in buffer containing 100 mM of glucose and 100 mM of glycerol for co-factor regeneration through *E. coli*'s native metabolism. Although endogenous cofactors were present in the CFEs, the reactions were supplemented with 1 mM of NADH, as previous studies indicated this as a limiting factor. Reactions were performed essentially as 2 liquid-phase reactions as the substrate, *n*-octane, was added in excess (250 μL). Unfortunately, hydroxylation activity was significantly lower than previously observed with CYP153A6 and CYP153A13 under similar conditions, with less than 0.5 mM of 1-octanol formed after 24 h. The low activity was attributed to the concentration of soluble FdR-A71 in the CFEs, resulting in insufficient electron transfer to CYP153A71. To improve the delivery of the reducing equivalents to CYP153A71 from NADH, various combinations of surrogate redox partners from CYP153A6 and CYP153A13 were evaluated with CYP153A71 for the hydroxylation of *n*-octane. The activity of CYP153A71 could be reconstituted through either a combination of the native pairing of Fdx and FdR from *Mycobacterium* (A6) or *A. borkumensis* (A13), or a mixed pairing (Figure 2). Similarly, both the surrogate FdRs could be combined with the native Fdx-A71 for activity. In all these instances, the activity significantly increased, with the greatest activity observed with the combination of CYP153A71 and FdR-A13, with either Fdx-A13 or Fdx-A71 (Figure 2). Not surprisingly, the Fdx and FdR from *A. dieselolei* showed a higher amino-acid-sequence identity with those of *A. borkumensis* (82% and 75%, respectively) than those of *Mycobacterium* (less than 50%). This productive intra-genus coupling of redox partners would suggest that the observed sequence divergence (*ca.* 20%) did not adversely affect the sites of protein–protein interaction required for electron shuttling. Additionally, the N-terminal His-tags did not prevent productive coupling between the redox partners or between the redox partners and the CYP.
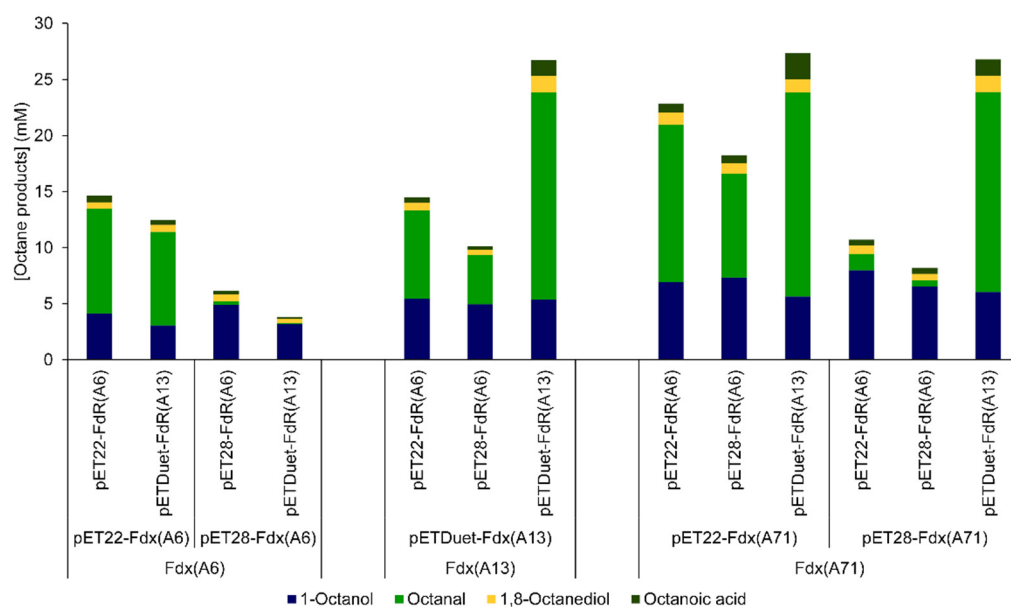
Figure 2. Hydroxylation of *n*-octane by CYP153A71 reconstituted with surrogate redox partners from CYP153A6 (Fdx-A6 and FdR-A6), expressed in pET22b(+) or pET28b(+), and the redox partners of CYP153A13 (Fdx-A13 and FdR-A13) expressed in pETDuet, or native Fdx (Fdx-A71) with surrogate FdRs.

Sequential over-hydroxylation was observed with the increased activity of CYP153A71, despite the *n*-octane being added in excess. Additional products observed included octanal, octanoic acid, as well as 1,8-octanediol. The further oxidation of terminal alcohols to their corresponding aldehydes and acids has often been attributed to endogenous oxidases in *E. coli*. However, the high concentrations of aldehydes and acids observed relative to control reactions containing only *E. coli* proteins suggested a second hydroxylation of the 1-alkanol to form a geminal diol (*gem*-diol) that spontaneously dehydrated to the aldehyde, which, in turn, can again be hydroxylated to the acid.

2.3. Substrate Scope

CYP153A71 was reconstituted with its native Fdx-A71 and the FdR from *A. borkumensis*, FdR-A13, (all expressed as His-tagged variants), and was subsequently used in comparative biotransformations of medium-chain *n*-alkanes (C8–C12). The well-characterized CYP153A6 and CYP153A13 hydroxylases were also included for comparison. As the biotransformation mixtures were prepared using equal volumes from constant wet biomass concentrations (0.12 g of wet-cell weight per 1 mL of biotransformation mixture), the final CYP concentrations in the reactions varied between CYPs due to expression levels. This, however, did not seem to be the most important factor in final-product yields (vide infra), but rather the ratio of CYP to their redox-partner proteins and co-factor regeneration.

Similar to CYP153A13, CYP153A71 displayed very high regioselectivity (>99%) for the terminal carbon of the tested *n*-alkanes. This contrasted with CYP153A6, which also catalyzed the sub-terminal hydroxylation of *n*-alkanes at the C2 position. The primary alcohols were rapidly over-hydroxylated to the aldehydes (and further to the corresponding acids), especially with CYP153A71 and CYP153A13 compared to CYP153A6. Although aldehydes are often observed in CYP153-catalyzed hydroxylations, their significance is often underestimated due to their poor extraction compared to alkanols (Figure S2) and the assumption that endogenous *E. coli* dehydrogenases or oxidases catalyzes their conversion from the alkanols. Unlike the closely related CYP153A13, CYP153A71 displayed a higher preference for *n*-octane than *n*-decane (Figure 3). Both these CYP153s still displayed a significant conversion of *n*-dodecane, compared to CYP153A6 that formed less than 1 mM of total products from *n*-dodecane. CYP153A71 also catalyzed diterminal hydroxylations of *n*-

alkanes to α,ω-diols. This has previously been observed with CYP153A16 and CYP153A34 from *n*-alkanes and the corresponding 1-alkanols at low substrate loadings [15], and more recently from 1-dodecanol by an engineered CYP153A33 variant for the production of α,ω-dodecanediol [28].
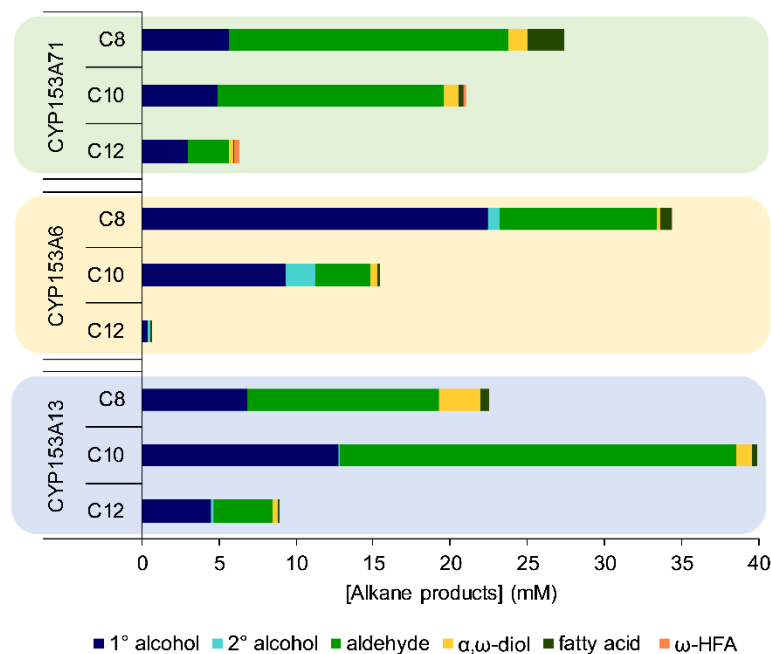

Figure 3. Comparative biotransformations of C8–C12 *n*-alkanes by CYP153A71, CYP153A6, and CYP153A13. Results are averages from two independent experiments, each with three biological replicates. *n*-alkanes added as a second phase (250 μL).

Intrigued by the high level of over-hydroxylation by CYP153A71 in the presence of excess *n*-alkanes, we explored its activity towards medium-chain alkanols and fatty acids. As previous reports have shown the decreased stability of CYP153s at higher 1-octanol concentrations [8], reactions were performed with alkanol concentrations of only 50 mM. Despite a decrease in the overall activity, all the CYP153s readily converted the 1-alkanols to their corresponding aldehydes, fatty acids, and α-ω-diols (Figure 4a). C10 and C12 hydroxy fatty acids were also observed with CYP153A71 and CYP153A13, with higher concentrations observed for 1-dodecanol. While CYP153A71 preferred the C8 *n*-alkane over the C10 and C12 *n*-alkanes, both CYP153A71 and CYP153A13 showed higher conversions with the C10 primary alcohol. The ratio of α,ω-diol to aldehyde also increased with the increasing chain length, with 1,12-dodecanediol as the major product formed by all three CYP153s. While CYP153A6 was the least prone to aldehyde production from *n*-alkanes, its activity was comparatively even lower when the 1-alkanols were added as substrates. This could potentially be due to the previously mentioned instability of CYP153A6 at high alkanol concentrations. The higher activities displayed by all three CYP153s towards 1-alkanols produced from *n*-alkanes compared to those added as substrates could be because the solubility of the alkanols in the *n*-alkane second phase decreased the effective concentration in the aqueous phase, potentially decreasing the deleterious effect of the alkanols to CYP activity. Alternatively, the higher aldehyde concentrations observed when starting from *n*-alkanes could be due to the formed 1-alkanols remaining in the active site and immediately hydroxylated to the aldehydes [29]. This would also explain why relatively more α,ω-diols were observed when the starting material was 1-alkanols.
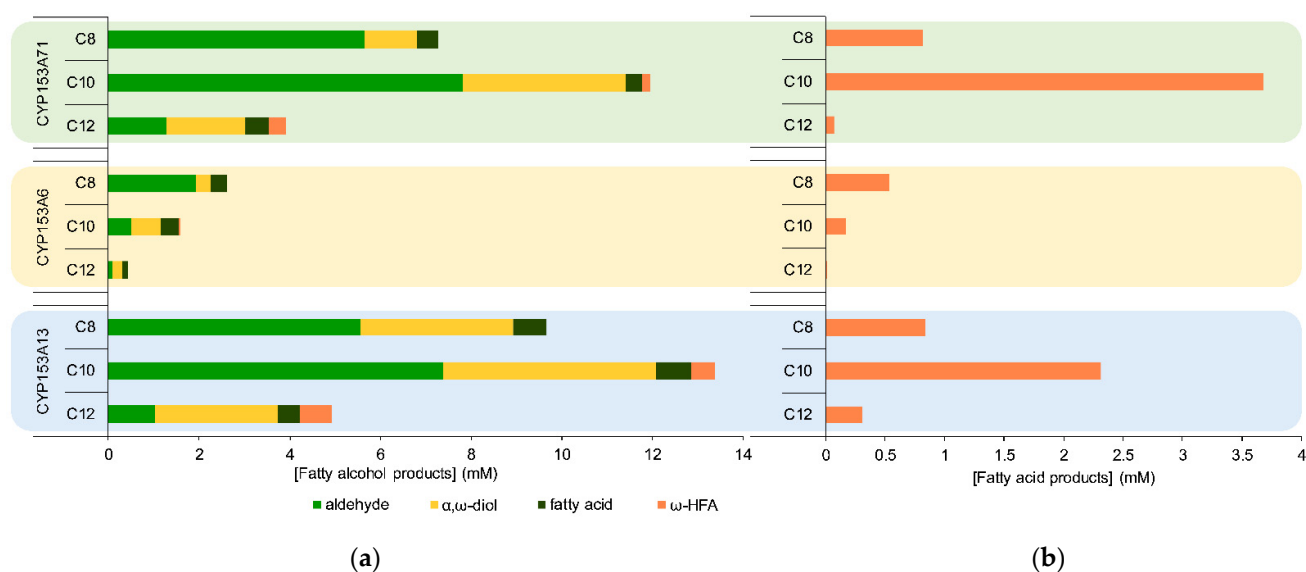
(a)   **(b)**

Figure 4. Comparative biotransformations of (**a**) C8–C12 1-alkanols (50 mM) and (**b**) C8–C12 fatty acids (20 mM) by CYP153A71, CYP153A6, and CYP153A13 Results are averages from two independent experiments, each with three biological replicates.

Lastly, the activity of CYP153A71 towards saturated fatty acids (C8-C12) was evaluated. Chain-length preference mirrored that observed for 1-alkanols, with CYP153A71 and CYP153A13 showing the highest conversion rates with decanoic acid and CYP153A6 with octanoic acid (Figure 4b). Only ω-hydroxy fatty acids were observed as products, with no over-hydroxylation to the diacids. Under these un-optimized reaction conditions, CYP153A71 produced *ca*. 1 mM of 8-hydroxyoctanoic acid and more than 3.5 mM of 10-hydroxydecanoic acid. CYP153A13 has previously been shown to catalyze the terminal hydroxylation of C12 to C16 saturated fatty acids [30]. A CYP153 variant (CYP153A33_Q129R/V141L/M228T) engineered for the terminal hydroxylation of medium-chain fatty acids was recently reported, achieving 0.24 mM of 8-hydroxyoctanoic acid from 1 mM of octanoic acid after 1 h and 1 μM of CYP [23]. CYP153A7_D258E showed complete conversion of 1 mM of octanoic acid after 4 h when using 1 μM of CYP [24]. A native CYP153 (CYP153AL.m from *Limnobacter*) has been reported for the effective production (*ca*. 15 mM) of 12-hydroxydodecanoic acid from the corresponding acid using resting whole cells of *E. coli* co-expressing a fatty acid transporter and its own redox partners [31].

2.4. Factors Affecting Over-Hydroxylation

To ensure that over-hydroxylation could be attributed to the CYP153 system and not endogenous *E. coli* proteins, CYP153A71, together with its native Fdx and FdR-A13 were purified to homogeneity for biotransformation reactions. We previously demonstrated through the deconstruction of the three-component CYP153A6 system that the Fdx concentration/ratio to CYP153 and FdR significantly influences product-formation rates and yields [32]. CYP153A71 was thus reconstituted using purified enzymes of CYP153A71:FdR:Fdx in a 1:1:60 molar ratio, and the ratios of the major products (1-octanol and octanal) were compared. Co-factor regeneration was performed using the glucose dehydrogenase from *Bacillus megaterium* (*Bm*GDH) and 0.1 mM of NADH with excess glucose (100 mM). Low product yields (<3 mM of total products) were produced when compared to using the enzymes added as CFEs (Figure 5a). Moreover, increasing the CYP153A71 concentration (up to 4 μM) did not significantly influence the total conversion. Nevertheless, significant amounts of octanal were still observed, confirming CYP153A71's role in sequential hydroxylation. The addition of proteins, such as bovine serum albumin (BSA) or protein extracts from *E. coli* (CFEs), has been shown to increase the activity and stability of CYP153A6 [32]. Therefore, the FdR and Fdx components were added as

CFEs to the purified CYP153A71 (Figure 5b). No additional GDH was added, with only endogenous *E. coli* metabolism used for cofactor regeneration. The overall activity (total products formed) significantly increased, together with an increased ratio of octanal to 1-octanol. Again, no differences were observed between reactions containing 1 or 4 µM of CYP. However, when GDH was added to aid co-factor regeneration, not only did the hydroxylation activity substantially increase, but the degree of over-hydroxylation to the aldehyde also increased with the increasing CYP concentration.
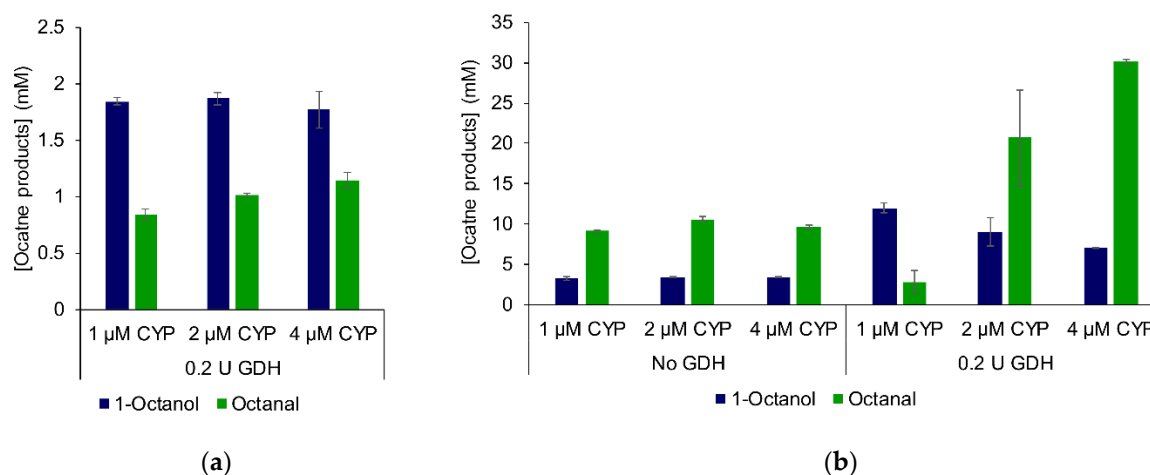

(**a**)

(**b**)

Figure 5. (**a**) Biotransformation of *n*-octane using purified CYP153A71 (1–4 µM), FdR-A13 (1 µM), Fdx-A71 (60 µM), and glucose dehydrogenase (GDH, 0.2 U mL^{-1}) for co-factor regeneration; (**b**) biotransformation of *n*-octane with purified CYP153A71 with Fdx-A71 and FdR-A13 added as cell-free extracts (CFEs). Reactions were performed with either glucose dehydrogenase (GDH, 0.2 U mL^{-1}) or no additional co-factor regeneration.

2.5. CYP153A71 Structure Determination

CYP153A71 was purified to homogeneity using immobilized metal affinity and gel-filtration chromatography (Figure S1). Characteristic red crystals grew within days, but diffracted poorly despite numerous attempts at optimization. Additionally, large contiguous stretches of electron density were either poor or absent, including the F and G helices as well as the F/G and B/C loops. This type of extreme structural plasticity has previously been observed with some CYP153s [33] and, in combination with only low-resolution data, made density interpretation problematic. We, therefore, turned to co-crystallizing CYP153A71 with octanoic acid. This not only improved the diffraction resolution to 1.95 Å (Table S1), but also resolved most of the density of the previously disordered regions. CYP153A71 crystallized in space group *P*2$_1$, with two copies in the asymmetric unit cell (ASU). Continuous electron density was observed for residues 48–470. The first 47 residues, as well as the N-terminal His-tag and thrombin cleavage site, were not modeled due to a lack of electron density. CYP153A71 displayed the overall canonical CYP450 fold (Figure 6a) with CYP153A33 from *Marinobacter aquaeolei* as the closest structural homologue (81% sequence identity, r.m.s.d. of 0.461 Å main-chain atoms). Octanoic acid could be modeled above the distal side of the heme and in one of the copies in the ASU did not displace the axial water molecule (chain A, Figure 6b). Although difference density could be observed above the heme in chain B, this would place the water molecule too close to the octanoic acid (vide infra). The two copies in the ASU could, however, be superimposed without any significant differences in the backbone conformation. The octanoic acid ligands were refined in two different conformations and only at 0.8 occupancy (Figure S4). As the overall density and B factors for chain A were better, it was used for a further comparison.
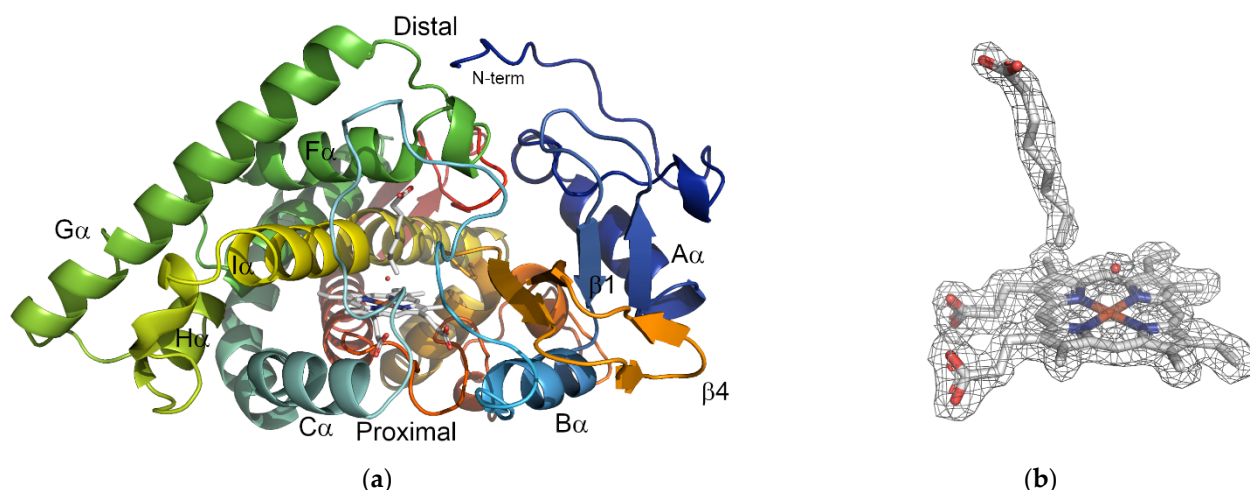
(**a**)

(**b**)

Figure 6. (**a**) Overall fold of CYP153A71 colored blue (N-terminus) to red (C-terminus). Numbering of helices and strands according to CYP101A1 (P450cam); (**b**) octanoic acid bound on the proximal side of the heme in chain A. Fe-coordinated water is shown as a red sphere. Electron density is displayed as mesh contoured at σ = 1 from a 2Fo-Fc map.

The surface rendering of the active site shows the tapering of the active-site tunnel as it approaches the heme (Figure 7). Except for T311, which forms part of the catalytic alcohol–acid pair (D310–T311), and M357, the residues in close contact with the methyl end (C8-C7) are non-polar. A comparison to CYP153A33 reveals these residues to be absolutely conserved (Figure S5). Similarly, the second-sphere residues from the heme, contacting C6-C4 are also conserved between CYP153A71 and CYP153A33. Again, apart from D310 (from the alcohol-acid pair) and a single methionine (M143) all are non-polar.
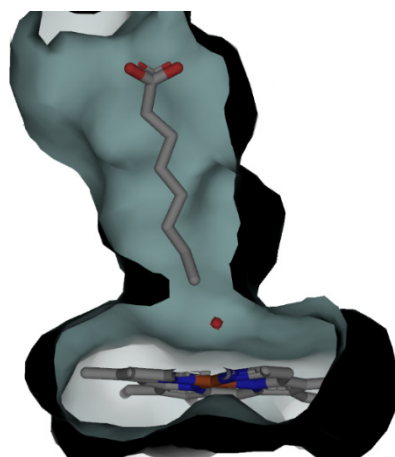

Figure 7. Surface rendering of CYP153A71 with bound *n*-octanoic acid displaying the tapered active-site substrate-access channel.

To date, no CYP153A has been crystallized with a physiological substrate (*n*-alkane). CYP153A33 is also the only member from this class of CYPs to have been co-crystallized with 12-hydroxydodecanoic acid [19]. A structural overlay of CYP1533A33 and CYP153A71 shows the octanoic acid and 12-hydroxydodecanoic acid to occupy the same position (Figure 8). However, whereas the octanoic acid did not displace the heme-coordinated water molecule, the terminal hydroxyl group of 12-hydroxydodecanoic acid displaced the axial water and was within coordination distance from the heme iron (2.3 Å). The distance between the difference density and terminal methyl group of octanoic acid in chain B could suggest potential product formation due to X-ray cryo-reduction leading to oxygenation [34]. In CYP153A33, the carboxyl group of 12-hydroxydodecanoic acid

was within bonding distance of a glutamine (Q133) and the backbone amide nitrogen of V145, both from the B/C loop [19]. This glutamine is conserved in CYP153A71 (Q129), with *n*-octanoic acid's carboxyl group also within close proximity to the glutamine. This type of substrate anchoring has been used to improve the catalytic efficiency of CYP153s towards fatty acid substrates [19,23]. The more polar residues observed closer to the surface of the protein in the third sphere could explain the higher activity with C10 alcohols and acids.
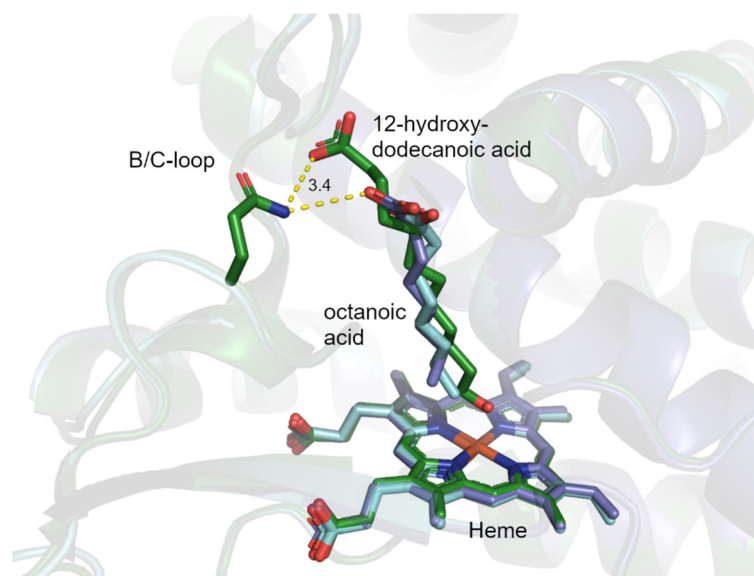

Figure 8. Overlay of CYP153A71 chain A (purple), chain B (blue), and CYP153A33 (green, 5FYG) showing the coordination of the carboxyl group of octanoic acid in CYP153A71 and 12-hydroxydodecanoic acid in CYP153A33 by the conserved Gln.

CYP52s, the eukaryotic counterparts of CYP153s in fungi, also catalyze the terminal hydroxylation of alkanes and fatty acids of various chain lengths. Unfortunately, no structural data are available for a member of the CYP52 family. However, a crystal structure of a mammalian CYP4 (CYP4B1), which has been shown to catalyze the terminal hydroxylation of *n*-alkanes, has been solved with bound *n*-octane [35]. One of the best-studied CYP450s is CYP102A1 from *Bacillus megaterium* (P450BM3), which catalyzes the sub-terminal hydroxylation of fatty acids [36]. Recently, the structure of its fungal counterpart, CYP505A30, was solved with dodecanoic acid in the active site [37]. However, neither protein nor variant thereof has been co-crystallized with a fatty acid that is within catalytic range of the heme. A structural overlay of CYP153A71, CYP4B1 with bound *n*-octane, CYP102A1 with bound N-palmitoylglycine (NPG) [38], and CYP505A30 with bound dodecanoic acid shows the different approaches and angles of the substrates relative to the heme (Figure 9). Whereas the substrate approach in CYP153s is more perpendicular to the heme, the approach of *n*-octane in CYP4B1 is more diagonal, and the terminal parts of the substrates in CYP102A1 and CYP505A30 are positioned parallel to the heme. The carboxyl groups of octanoic acid and 12-hydroxydodecanoic acid in CYP153A71 and CYP153A33 mainly interact with the unstructured B/C loop, whereas the *n*-octane in CYP4B1, the NPG in CYP102A1, and dodecanoic acid in CYP505A30 are positioned closer to the β5 hairpin. CYP4B1, CYP102A1, and CYP505A30 form α-helices at the top of the B/C loop. This bulkier structure (B′-helix) potentially forces the positioning of the substrates towards a more diagonal approach. Different substrate access channels have been proposed for various CYPs [39]. Substrate access in CYP153A71 is potentially mediated via the unstructured B/C loop, as the N-terminus lies on top of the F/G loop, whereas the F and G helices and the associated F/G loop have been shown to significantly alter positions in the substrate-free and bound forms [40]. The importance of the B/C loop is motivated further by the structures of CYP153A33, where the

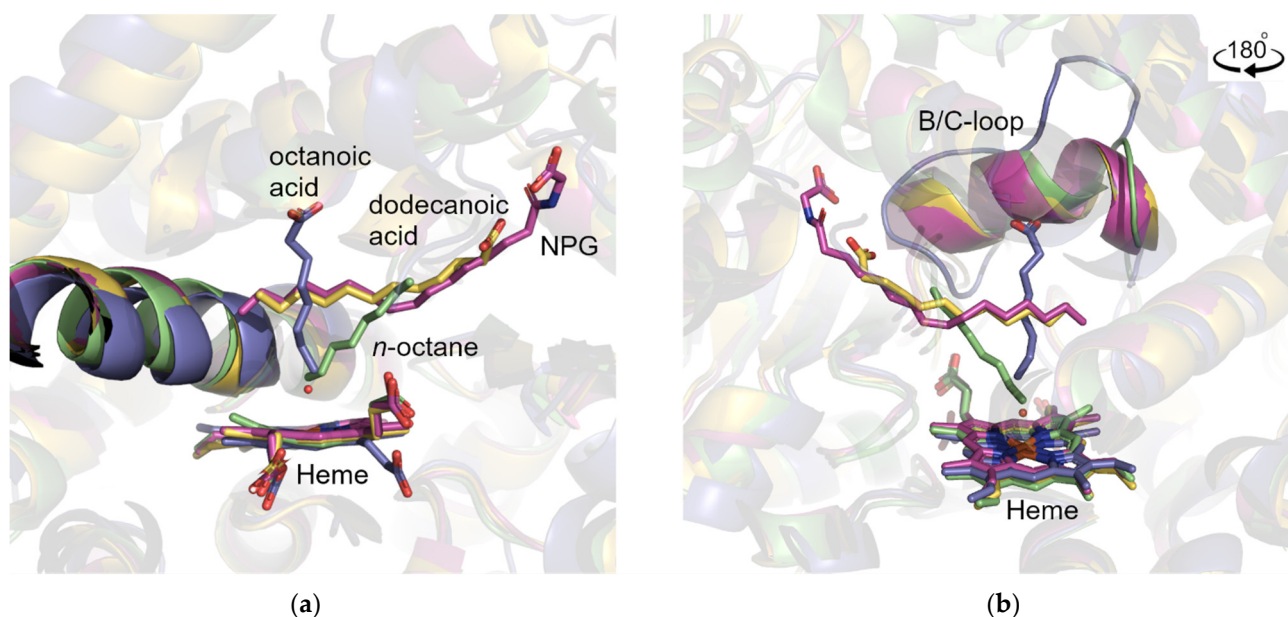F/G helices and F/G loop occupy the same space in both the structures with and without substrates [19].

(**a**)   (**b**)

Figure 9. (**a**) Substrate binding relative to I-helix and heme by CYP153A71 (blue, octanoic acid), CYP4B1 (green, *n*-octane, 5T6Q), CYP102A1 (pink, N-palmitoylglycine, 3CBD), and CYP505A30 (yellow, dodecanoic acid, 7P6L); (**b**) substrate binding (rotated 180 °C) relative to B/C loop.

3. Materials and Methods

3.1. Expression Constructs

A. dieselolei B-5 and *A. borkumensis* SK2 strains were obtained from the DSMZ, and genomic DNA (gDNA) was isolated using the Quick-DNA Fungal/Bacterial Microprep Kit (Zymo Research) as per the manufacturer's instructions. Genes encoding CYP153A71 and its associated redox-partner proteins (Fdx-A71 and FdR-A71) were identified in the genome of *A. dieselolei* B-5 by BLAST analysis using the CYP153A13 from *A. borkumensis* SK2 as the query. The redox partners were identified in the upstream and downstream flanking regions of CYP153A71, respectively. The genes were PCR-amplified (Table S2) from gDNA using KOD Hot Start DNA polymerase (Novagen), where the amplicons were then phosphorylated followed by blunt-end ligation into pSMART HCKan (Lucigen). The open reading frames of CYP153A71 and FdR-A71 were sub-cloned to pET22b(+) and pET28b(+) (Novagen) via *Nde*I and *Sal*I, whereas Fdx-A71 was sub-cloned to the same vectors using *Nde*I and *Xho*I. CYP153A13 was PCR-amplified from the previously described artificial-fusion construct, pET28:CYP153A13_RhFRed [41], and sub-cloned to pET22b(+) and pET28b(+) via *Nde*I and *Hind*III. Ferredoxin (Fdx-A13) and ferredoxin reductase (FdR-A13) were PCR-amplified from gDNA and ultimately sub-cloned to pETDuet-1 via *Nde*I and *Avr*II. FdR-A13 was also sub-cloned to pET28 via *Nde*I and *Avr*II/*Nhe*I compatible sticky ends to create an N-terminally His-tagged variant for purification. The expression constructs of CYP153A6 and its associated FdR and Fdx were as previously described [32]. The glucose dehydrogenase from *Bacillus megaterium* (*Bm*GDH) was kindly provided by Prof. Dirk Holtmann (then at Dechema, Germany) and sub-cloned to pET28b(+), as previously described [32].

3.2. Heterologous Expression

The expression constructs were transformed into BL21-Gold(DE3) (Stratagene) and selected on LB-agar plates containing either 30 µg mL^{-1} of kanamycin (pET28b(+)) or 100 µg mL^{-1} of ampicillin (pET22b(+)/pETDuet-1). Inoculums (5 mL) were prepared in LB medium (37 °C, overnight with shaking) containing the same antibiotics. Heterologous

expression was performed using autoinduction (ZYP5052) medium [42] with the appropriate antibiotic. For CYP153 expression, ZYP5052 media was also supplemented with 0.5 mM δ-aminolevulinic acid hydrochloride and 0.05 mM $FeCl_3$. The cells were incubated at 20 °C with shaking (200 rpm) for 48 h and harvested by centrifugation ($7000 \times g$, 10 min, 4 °C). Protein expression was evaluated using SDS-PAGE analysis of the cell-free extracts, as described below. The CYP153 concentrations were determined with CO-difference spectra [43] in microtiter plates (200 μL), as previously described [41], using an extinction coefficient of 91 mM^{-1} cm^{-1} at 450 nm.

3.3. Biotransformations Using Cell-Free Extracts (CFEs)

For the biotransformations, cells were resuspended in 200 mM Tris-HCl buffer (pH 8) containing 100 mM of glucose and 100 mM of glycerol (1 g of wet-cell weight per 5 mL of buffer). The resuspended cells were lysed by a single passage through a One-Shot Cell Disruptor (Constant Systems) at 30 kPsi. Unbroken cells and insoluble debris were removed by centrifugation ($12,000 \times g$, 30 min, 4 °C) to yield the cell-free extract (CFE). Biotransformations (1 mL) were performed in 40 mL amber, glass vials containing 0.4 mL of buffer (200 mM Tris-HCl pH 8, containing 100 mM of glucose and 100 mM of glycerol), 1 mM of NADH, and equal volumes (0.2 mL) of CFEs from a CYP153 candidate and their respective redox partners (FdR and Fdx). Reactions were initiated by the addition of *n*-alkanes (C8–C12) as a second phase (250 μL) or 50 mM of the corresponding 1-alkanol (added from 500 mM of stock solution in ethanol) or 10 mM of fatty acid (added from 100 mM of stock solution in DMSO). Reactions were prepared in triplicate and incubated for 24 h at 20 °C with shaking (200 rpm).

The reaction mixtures were extracted using 1 mL (2×0.5 mL) of ethyl acetate containing 2 mM of 1-undecanol as an internal standard. An additional 170 μL of 5 M HCl was added to the reaction mixtures to facilitate the extraction of the fatty acids. Trimethylsulfonium hydroxide (TMSH) was used for methylation to facilitate the analysis of the fatty acids. The products were analyzed by gas chromatography (GC-FID) using a Shimadzu GC-2010 equipped with a FactorFour VF-5ms column (Agilent, 60 m $\times$ 0.32 mm $\times$ 0.25 μm). The products were identified through a comparison with authentic standards and quantified using extracted standards (from biotransformation buffers) to represent the concentrations present in the reaction mixtures.

3.4. Protein Purificaton

For purification, the cells were resuspended in immobilized metal-affinity chromatography (IMAC) binding buffer (50 mM Tris-HCl pH 7.4, 500 mM NaCl, and 40 mM imidazole). Cells lysis and CFE preparation were as described above. Further cell debris was removed from the CFE by ultracentrifugation ($90,000 \times g$ for 90 min, 4 °C). The clear lysates were loaded on a 5 mL HisTrap FF (GE Healthcare) nickel affinity column equilibrated with the IMAC buffer. Unbound proteins were eluted from the column with 10 column volumes (50 mL) of the same buffer. Bound proteins were eluted with a linear gradient of increasing imidazole concentration (50 mM Tris pH 7.4, 500 mM NaCl, and 40–500 mM imidazole). Fractions containing the proteins of interest were pooled and concentrated to *ca*. 2.5 mL using ultrafiltration (Amicon centrifugal unit (10 or 30 kDa MWCO)). For the biotransformations, concentrated proteins were desalted using PD-10 columns (GE Healthcare) equilibrated with 20 mM Tris-HCl buffer (pH 8) containing 10 mM of NaCl. For crystallization, the concentrated CYP153A71 protein was purified further using size-exclusion chromatography (SEC) using a Sephacryl HR-200 size-exclusion column (GE Healthcare) in the same buffer described above. Protein concentration was determined using the Pierce BCA kit (Thermo Scientific) with bovine serum albumin (BSA) as a standard.

3.5. Biotransformations Using Purified Enzyme

CYP153A71, Fdx-A71, FdR-A13, and *Bm*GDH were purified using IMAC and SEC as described above. Biotransformations were performed in 200 mM Tris-HCl (pH 8) buffer

containing 100 mM of glucose and 100 mM of glycerol; 1–4 µM CYP153A71; 60 µM Fdx-A71 and 1 µM FdR-A13; 0.1 mM NADH; and 0.2 U mL^{-1} *Bm*GDH. Alternatively, purified CYP153A71 (1–4 µM) was combined in the same buffer with 200 µL of CFE of FdR-A13 and Fdx-A71 (each contributing 0.04 g$_{WCW}$ mL$_{BRM}$$^{-1}$), and 0.1 mM of NADH with or without 0.2 U mL^{-1} *Bm*GDH.

3.6. Crystallization and Structure Determination of CYP153A71

CYP153A17 was co-crystallized with 10 mM of octanoic acid by vapor diffusion using equal volumes of protein (1 µL, 6–8 mg mL^{-1}) and 0.1 M of HEPES buffer (pH 7.5) containing 12% (*w/v*) polyethylene glycol (PEG) 3350 as a precipitant. Crystals were briefly soaked in precipitant solution containing 30% *w/v* glycerol before cryocooling in liquid nitrogen. X-ray diffraction data were collected at Diamond Light Source (UK) at beamline i03. The data were indexed and integrated using AutoPROC [44], and scaled and merged using POINTLESS [45] and AIMLESS [46]. Molecular replacement was performed with Phaser [47] using CYP153A33 [19] as a search model (PDB ID: 5FYF). The structure was refined by iterative cycles of manual building in Coot [48] and automatic refinement in REFMAC5 [49]. The structure was validated using the multimeric validation program from the CCP4 suite [50], including MolProbity [51]. Figures were generated in Pymol [52]. Coordinates and structure factors were deposited in the Protein Data Bank (PDB) under 8B2P.

4. Conclusions

CYP153A71 from *A. dieselolei* B-5 can be heterologously produced in *E. coli* at high yields. Its activity can be reconstituted with either surrogate redox-partner proteins, Fdx-A13 and FdR-A13 from *A. borkumensis* SK2, or its native Fdx-A71 and the surrogate FdR-A13. CYP153A71 catalyzes the terminal hydroxylation of C8–C12 *n*-alkanes, with a preference for *n*-octane. Despite the natural substrates (*n*-alkanes) added in excess, the produced 1-alkanols were over-oxidized by CYP153A71 to the corresponding aldehydes, fatty acids, as well as α,ω-diols, with the aldehydes being the major products produced from *n*-octane and *n*-decane, the preferred substrates. The ratio of α,ω-diols to aldehydes can, however, be improved by utilizing 1-alkanols as the starting material. Additionally, CYP153A71 catalyzed the ω-hydroxylation of C8–C12 fatty acids. Under these unoptimized conditions, concentrations of *ca.* 1 mM of 8-hydroxyoctanoic acid and more than 3.5 mM of 12-hydroxydodecanoic acid were achieved, rivalling CYP153s that were evolved for fatty acid hydroxylation. The structural analysis of CYP153A71 through X-ray crystallography displayed a tapered hydrophobic active site, which allowed only the terminal methyl group of the bound octanoic acid to approach the heme. In CYP153A71, as in CYP153A33, the approach of the alkyl chain was more perpendicular to the heme, whereas in structures of the sub-terminal fatty acid hydroxylases, CYP02A1 and CYP505A30, substrate approach was diagonal with the terminal and sub-terminal carbons of the alkyl chain finally positioned parallel to and outside the catalytic range of the heme. CYP153A71, similar to CYP153A33, also differed from the sub-terminal hydroxylases in that the B/C loop in CYP153A71 did not form a secondary structure, but a random coil. The B/C loop was not only important as an access channel, but also as a potential anchoring point for charged or polar groups of substrates. The high activity observed with CYP153A71 makes this enzyme an ideal candidate for future directed evolution studies to improve and expand the substrate scope for the production of 1-alkanols, α,ω-diols, and ω-hydroxy fatty acids.

Supplementary Materials: The following supporting information can be downloaded at: https://www.mdpi.com/article/10.3390/catal12101213/s1, Figure S1: SDS-PAGE analysis of redox-partner proteins of CYP153A6 and CYP153A13; Figure S2: comparative GC-FID chromatograms showing the extraction efficiency of hydroxylated products obtained from *n*-octane; Figure S3: SDS-PAGE analysis of purified CYP153A71; Figure S4: Overlay of CYP153A71 chain A (blue) and chain B (gray) showing the two different orientations of octanoic acid. Figure S5: (a) Overlay of CYP153A71 chain A (blue) and CYP153A33 (green, 5FYG) showing the amino acids lining the active sites. Numbering is that of

CYP153A71 with I130 adopting a different conformation from that observed in CYP153A33. *L228 from the F-helix is a methionine in CYP153A33. (b) View rotated 90°. Table S1: data collection and refinement statistics for CYP153A71; Table S2: targeted genes from *A. dieselolei* B-5 and *A. borkumensis* SK2. Table S3: Percentage amino acid sequence identity between different CYP153A.

Conflicts of Interest: The authors declare no conflict of interest. The funders had no role in the design of the study; in the collection, analyses, or interpretation of data; in the writing of the manuscript; or in the decision to publish the results.

References

1. Sterckx, H.; Morel, B.; Maes, B.U.W. Catalytic Aerobic Oxidation of C(Sp^3)−H Bonds. *Angew. Chem. Int. Ed.* **2019**, *58*, 7946–7970. [CrossRef]
2. Münch, J.; Püllmann, P.; Zhang, W.; Weissenborn, M.J. Enzymatic Hydroxylations of Sp^3-Carbons. *ACS Catal.* **2021**, *11*, 9168–9203. [CrossRef]
3. Guengerich, F.P. Mechanisms of Cytochrome P450 Substrate Oxidation: MiniReview. *J. Biochem. Mol. Toxicol.* **2007**, *21*, 163–168. [CrossRef] [PubMed]
4. Hammerer, L.; Winkler, C.K.; Kroutil, W. Regioselective Biocatalytic Hydroxylation of Fatty Acids by Cytochrome P450s. *Catal. Lett.* **2018**, *148*, 787–812. [CrossRef]
5. Hannemann, F.; Bichet, A.; Ewen, K.M.; Bernhardt, R. Cytochrome P450 Systems-Biological Variations of Electron Transport Chains. *Biochim. Biophys. Acta* **2007**, *1770*, 330–344. [CrossRef]
6. Van Beilen, J.B.; Funhoff, E.G.; van Loon, A.; Just, A.; Kaysser, L.; Bouza, M.; Holtackers, R.; Röthlisberger, M.; Li, Z.; Witholt, B. Cytochrome P450 Alkane Hydroxylases of the CYP153 Family Are Common in Alkane-Degrading Eubacteria Lacking Integral Membrane Alkane Hydroxylases. *Appl. Environ. Microbiol.* **2006**, *72*, 59–65. [CrossRef] [PubMed]
7. Van Beilen, J.B.; Holtackers, R.; Lüscher, D.; Bauer, U.; Witholt, B.; Duetz, W.A. Biocatalytic Production of Perillyl Alcohol from Limonene by Using a Novel *Mycobacterium* sp. Cytochrome P450 Alkane Hydroxylase Expressed in *Pseudomonas Putida*. *Appl. Environ. Microbiol.* **2005**, *71*, 1737–1744. [CrossRef] [PubMed]
8. Gudiminchi, R.K.; Randall, C.; Opperman, D.J.; Olaofe, O.A.; Harrison, S.T.L.; Albertyn, J.; Smit, M.S. Whole-Cell Hydroxylation of n-Octane by *Escherichia coli* Strains Expressing the CYP153A6 Operon. *Appl. Microbiol. Biotechnol.* **2012**, *96*, 1507–1516. [CrossRef] [PubMed]
9. Funhoff, E.G.; Salzmann, J.; Bauer, U.; Witholt, B.; van Beilen, J.B. Hydroxylation and Epoxidation Reactions Catalyzed by CYP153 Enzymes. *Enzym. Microb. Technol.* **2007**, *40*, 806–812. [CrossRef]
10. Li, A.; Liu, J.; Pham, S.Q.; Li, Z. Engineered P450pyr Monooxygenase for Asymmetric Epoxidation of Alkenes with Unique and High Enantioselectivity. *Chem. Commun.* **2013**, *49*, 11572. [CrossRef] [PubMed]
11. Kubota, M.; Nodate, M.; Yasumoto-Hirose, M.; Uchiyama, T.; Kagami, O.; Shizuri, Y.; Misawa, N. Isolation and Functional Analysis of Cytochrome P450 CYP153A Genes from Various Environments. *Biosci. Biotechnol. Biochem.* **2005**, *69*, 2421–2430. [CrossRef] [PubMed]
12. Malca, S.H.; Scheps, D.; Kühnel, L.; Venegas-Venegas, E.; Seifert, A.; Nestl, B.M.; Hauer, B. Bacterial CYP153A Monooxygenases for the Synthesis of Omega-Hydroxylated Fatty Acids. *Chem. Commun.* **2012**, *48*, 5115. [CrossRef] [PubMed]
13. Funhoff, E.G.; Bauer, U.; García-Rubio, I.; Witholt, B.; van Beilen, J.B. CYP153A6, a Soluble P450 Oxygenase Catalyzing Terminal-Alkane Hydroxylation. *J. Bacteriol.* **2006**, *188*, 5220–5227. [CrossRef] [PubMed]

14. Fujii, T.; Narikawa, T.; Sumisa, F.; Arisawa, A.; Takeda, K.; Kato, J. Production of α,ω-Alkanediols Using *Escherichia coli* Expressing a Cytochrome P450 from *Acinetobacter* sp. OC4. *Biosci. Biotechnol. Biochem.* **2006**, *70*, 1379–1385. [CrossRef] [PubMed]

15. Scheps, D.; Malca, S.H.; Hoffmann, H.; Nestl, B.M.; Hauer, B.; Malca, S.H.; Hoffmann, H.; Nestl, B.M.; Hauer, B. Regioselective ω-Hydroxylation of Medium-Chain n-Alkanes and Primary Alcohols by CYP153 Enzymes from *Mycobacterium marinum* and *Polaromonas* sp. strain JS666. *Org. Biomol. Chem.* **2011**, *9*, 6727–6733. [CrossRef]

16. Yang, Y.; Liu, J.; Li, Z. Engineering of P450pyr Hydroxylase for the Highly Regio- and Enantioselective Subterminal Hydroxylation of Alkanes. *Angew. Chem. Int. Ed.* **2014**, *53*, 3120–3124. [CrossRef]

17. Nebel, B.A.; Scheps, D.; Malca, S.H.; Nestl, B.M.; Breuer, M.; Wagner, H.G.; Breitscheidel, B.; Kratz, D.; Hauer, B. Biooxidation of N-Butane to 1-Butanol by Engineered P450 Monooxygenase under Increased Pressure. *J. Biotechnol.* **2014**, *191*, 86–92. [CrossRef]

18. Yang, Y.; Chi, Y.T.; Toh, H.H.; Li, Z. Evolving P450pyr Monooxygenase for Highly Regioselective Terminal Hydroxylation of N-Butanol to 1,4-Butanediol. *Chem. Commun.* **2015**, *51*, 914–917. [CrossRef]

19. Hoffmann, S.M.; Danesh-Azari, H.R.; Spandolf, C.; Weissenborn, M.J.; Grogan, G.; Hauer, B. Structure-Guided Redesign of CYP153AM.Aq for the Improved Terminal Hydroxylation of Fatty Acids. *ChemCatChem* **2016**, *8*, 3178. [CrossRef]

20. Notonier, S.; Gricman, Ł.; Pleiss, J.; Hauer, B. Semirational Protein Engineering of CYP153A$_{M.Aq.}$-CPR$_{BM3}$ for Efficient Terminal Hydroxylation of Short- to Long-Chain Fatty Acids. *ChemBioChem* **2016**, *17*, 1550–1557. [CrossRef]

21. Duan, Y.; Ba, L.; Gao, J.; Gao, X.; Zhu, D.; de Jong, R.M.; Mink, D.; Kaluzna, I.; Lin, Z. Semi-Rational Engineering of Cytochrome CYP153A from *Marinobacter aquaeolei* for Improved ω-Hydroxylation Activity towards Oleic Acid. *Appl. Microbiol. Biotechnol.* **2016**, *100*, 8779–8788. [CrossRef] [PubMed]

22. Jung, E.; Park, B.G.; Yoo, H.W.; Kim, J.; Choi, K.Y.; Kim, B.G. Semi-Rational Engineering of CYP153A35 to Enhance ω-Hydroxylation Activity toward Palmitic Acid. *Appl. Microbiol. Biotechnol.* **2018**, *102*, 269–277. [CrossRef] [PubMed]

23. Rapp, L.R.; Marques, S.M.; Zukic, E.; Rowlinson, B.; Sharma, M.; Grogan, G.; Damborsky, J.; Hauer, B. Substrate Anchoring and Flexibility Reduction in CYP153A M.Aq Leads to Highly Improved Efficiency toward Octanoic Acid. *ACS Catal.* **2021**, *11*, 3182–3189. [CrossRef]

24. Dong, Y.; Chong, G.; Li, C.; Chen, Q.; Pan, J.; Li, A.; Xu, J. Carving the Active Site of CYP153A7 Monooxygenase for Improving Terminal Hydroxylation of Medium-Chain Fatty Acids. *ChemBioChem* **2022**, *23*, e202200063. [CrossRef]

25. Liu, C.; Wang, W.; Wu, Y.; Zhou, Z.; Lai, Q.; Shao, Z. Multiple Alkane Hydroxylase Systems in a Marine Alkane Degrader, *Alcanivorax dieselolei* B-5. *Environ. Microbiol.* **2011**, *13*, 1168–1178. [CrossRef]

26. Wang, W.; Shao, Z. The Long-Chain Alkane Metabolism Network of Alcanivorax Dieselolei. *Nat. Commun.* **2014**, *5*, 5755. [CrossRef]

27. Otomatsu, T.; Bai, L.; Fujita, N.; Shindo, K.; Shimizu, K.; Misawa, N. Bioconversion of Aromatic Compounds by *Escherichia coli* That Expresses Cytochrome P450 CYP153A13a Gene Isolated from an Alkane-Assimilating Marine Bacterium *Alcanivorax borkumensis*. *J. Mol. Catal. B Enzym.* **2010**, *66*, 234–240. [CrossRef]

28. Park, H.; Bak, D.; Jeon, W.; Jang, M.; Ahn, J.; Choi, K. Engineering of CYP153A33 with Enhanced Ratio of Hydroxylation to Overoxidation Activity in Whole-Cell Biotransformation of Medium-Chain 1-Alkanols. *Front. Bioeng. Biotechnol.* **2022**, *9*, 817455. [CrossRef]

29. Guengerich, F.P.; Sohl, C.D.; Chowdhury, G. Multi-Step Oxidations Catalyzed by Cytochrome P450 Enzymes: Processive vs. Distributive Kinetics and the Issue of Carbonyl Oxidation in Chemical Mechanisms. *Arch. Biochem. Biophys.* **2011**, *507*, 126–134. [CrossRef]

30. Jung, E.; Park, B.G.; Ahsan, M.M.; Kim, J.; Yun, H.; Choi, K.-Y.; Kim, B.-G. Production of ω-Hydroxy Palmitic Acid Using CYP153A35 and Comparison of Cytochrome P450 Electron Transfer System in Vivo. *Appl. Microbiol. Biotechnol.* **2016**, *100*, 10375–10384. [CrossRef]

31. Joo, S.Y.; Yoo, H.W.; Sarak, S.; Kim, B.G.; Yun, H. Enzymatic Synthesis of ω-Hydroxydodecanoic Acid by Employing a Cytochrome P450 from *Limnobacter* sp. 105 MED. *Catalysts* **2019**, *9*, 54. [CrossRef]

32. Kochius, S.; van Marwijk, J.; Ebrecht, A.C.; Opperman, D.J.; Smit, M.S. Deconstruction of the CYP153A6 Alkane Hydroxylase System: Limitations and Optimization of In Vitro Alkane Hydroxylation. *Catalysts* **2018**, *8*, 531. [CrossRef]

33. Fiorentini, F.; Hatzl, A.M.; Schmidt, S.; Savino, S.; Glieder, A.; Mattevi, A. The Extreme Structural Plasticity in the CYP153 Subfamily of P450s Directs Development of Designer Hydroxylases. *Biochemistry* **2018**, *57*, 6701–6714. [CrossRef]

34. Amaya, J.A.; Batabyal, D.; Poulos, T.L. Proton Relay Network in the Bacterial P450s: CYP101A1 and CYP101D1. *Biochemistry* **2020**, *59*, 2896–2902. [CrossRef] [PubMed]

35. Hsu, M.H.; Baer, B.R.; Rettie, A.E.; Johnson, E.F. The Crystal Structure of Cytochrome P450 4B1 (CYP4B1) Monooxygenase Complexed with Octane Discloses Several Structural Adaptations for ω-Hydroxylation. *J. Biol. Chem.* **2017**, *292*, 5610–5621. [CrossRef] [PubMed]

36. Whitehouse, C.J.C.; Bell, S.G.; Wong, L.L. P450 BM3 (CYP102A1): Connecting the Dots. *Chem. Soc. Rev.* **2012**, *41*, 1218–1260. [CrossRef] [PubMed]

37. Aschenbrenner, J.C.; Ebrecht, A.C.; Tolmie, C.; Smit, M.S.; Opperman, D.J. Structure of the Fungal Hydroxylase, CYP505A30, and Rational Transfer of Mutation Data from CYP102A1 to Alter Regioselectivity. *Catal. Sci. Technol.* **2021**, *11*, 7359–7367. [CrossRef]

38. Fasan, R.; Meharenna, Y.T.; Snow, C.D.; Poulos, T.L.; Arnold, F.H. Evolutionary History of a Specialized P450 Propane Monooxygenase. *J. Mol. Biol.* **2008**, *383*, 1069–1080. [CrossRef]

39. Urban, P.; Lautier, T.; Pompon, D.; Truan, G. Ligand Access Channels in Cytochrome P450 Enzymes: A Review. *Int. J. Mol. Sci.* **2018**, *19*, 1617. [CrossRef]

40. Li, H.; Poulos, T.L. The Structure of the Cytochrome P450BM-3 Haem Domain Complexed with the Fatty Acid Substrate, Palmitoleic Acid. *Nat. Struct. Biol.* **1997**, *4*, 140–146. [CrossRef]

41. Pennec, A.; Jacobs, C.L.; Opperman, D.J.; Smit, M.S. Revisiting Cytochrome P450-Mediated Oxyfunctionalization of Linear and Cyclic Alkanes. *Adv. Synth. Catal.* **2015**, *357*, 118–130. [CrossRef]

42. Studier, F.W. Protein Production by Auto-Induction in High Density Shaking Cultures. *Protein Expr. Purif.* **2005**, *41*, 207–234. [CrossRef] [PubMed]

43. Guengerich, F.P.; Martin, M.V.; Sohl, C.D.; Cheng, Q. Measurement of Cytochrome P450 and NADPH-Cytochrome P450 Reductase. *Nat. Protoc.* **2009**, *4*, 1245–1251. [CrossRef] [PubMed]

44. Vonrhein, C.; Flensburg, C.; Keller, P.; Sharff, A.; Smart, O.; Paciorek, W.; Womack, T.; Bricogne, G. Data Processing and Analysis with the AutoPROC Toolbox. *Acta Cryst.* **2011**, *D67*, 293–302.

45. Evans, P. Scaling and Assessment of Data Quality. *Acta Crystallogr. Sect. D Biol. Crystallogr.* **2006**, *62*, 72–82. [CrossRef] [PubMed]

46. Evans, P.R.; Murshudov, G.N. How Good Are My Data and What Is the Resolution? *Acta Crystallogr. Sect. D Biol. Crystallogr.* **2013**, *D69*, 1204–1214. [CrossRef] [PubMed]

47. McCoy, A.J.; Grosse-Kunstleve, R.W.; Adams, P.D.; Winn, M.D.; Storoni, L.C.; Read, R.J. Phaser Crystallographic Software. *J. Appl. Crystallogr.* **2007**, *40*, 658–674. [CrossRef] [PubMed]

48. Emsley, P.; Lohkamp, B.; Scott, W.G.; Cowtan, K. Features and Development of Coot. *Acta Crystallogr. Sect. D Biol. Crystallogr.* **2010**, *66*, 486–501. [CrossRef]

49. Murshudov, G.N.; Skubák, P.; Lebedev, A.A.; Pannu, N.S.; Steiner, R.A.; Nicholls, R.A.; Winn, M.D.; Long, F.; Vagin, A.A. REFMAC 5 for the Refinement of Macromolecular Crystal Structures. *Acta Crystallogr. Sect. D Biol. Crystallogr.* **2011**, *67*, 355–367. [CrossRef]

50. Winn, M.D.; Ballard, C.C.; Cowtan, K.D.; Dodson, E.J.; Emsley, P.; Evans, P.R.; Keegan, R.M.; Krissinel, E.B.; Leslie, A.G.W.; McCoy, A.; et al. Overview of the CCP 4 Suite and Current Developments. *Acta Crystallogr. Sect. D Biol. Crystallogr.* **2011**, *67*, 235–242. [CrossRef]

51. Chen, V.B.; Arendall, W.B.; Headd, J.J.; Keedy, D.A.; Immormino, R.M.; Kapral, G.J.; Murray, L.W.; Richardson, J.S.; Richardson, D.C. MolProbity: All-Atom Structure Validation for Macromolecular Crystallography. *Acta Crystallogr. Sect. D Biol. Crystallogr.* **2010**, *66*, 12–21. [CrossRef] [PubMed]

52. DeLano, W.L. PyMOL: An Open-Source Molecular Graphics Tool. *CCP4 Newsl. Protein Crystallogr.* **2002**, *40*, 82–92.